Graph Signal Processing of Low and High-Order Dynamic Functional Connectivity Networks Using EEG Resting-State for Schizophrenia: A Whole Brain Breakdown

Stavros I. Dimitriadis[1-6*]

1 Cardiff University Brain Research Imaging Centre, School of Psychology, Cardiff University, Cardiff, United Kingdom
2 Neuroinformatics Group, Cardiff University Brain Research Imaging Centre, School of Psychology, Cardiff University, Cardiff, United Kingdom
3 Division of Psychological Medicine and Clinical Neurosciences, School of Medicine, Cardiff University, Cardiff, United Kingdom
4 School of Psychology, Cardiff University, Cardiff, United Kingdom
5 Neuroscience and Mental Health Research Institute, School of Medicine, Cardiff University, Cardiff, United Kingdom
6 MRC Centre for Neuropsychiatric Genetics and Genomics, School of Medicine, Cardiff University, Cardiff, United Kingdom

*Corresponding author

Dr. Stavros I.Dimitriadis

Cardiff University Brain Research Imaging Centre, School of Psychology, Cardiff University, Cardiff, United Kingdom

Email: stidimitriadis@gmail.com / DimitriadisS@cardiff.ac.uk

Abstract:

Conventional static or dynamic functional connectivity graph (FCG/DFCG) referred to as low-order FCG focusing on temporal correlation estimates of the resting-state electroencephalography (rs-EEG) time series between any potential pair of brain areas. A DFCG is first constructed from multichannel recordings by adopting the methodology of sliding-window and a proper functional connectivity estimator. However, low-order FC ignores the high-level inter-relationship of brain areas. Recently, a high-order version of FCG has emerged by estimating the correlations of the time series that describe the fluctuations of the functional strength of every pair of ROIs across experimental time.

In the present study, a dynamic functional connectivity graph (DFCG) has been estimated using the imaginary part of phase lag value (iPLV). We analyzed DFCG profiles of electroencephalographic resting state (eyes-closed) recordings of healthy controls subjects (n=39) and subjects with symptoms of schizophrenia (n=45) in basic frequency bands $\{\delta,\theta,\alpha_1,\alpha_2,\beta_1,\beta_2,\gamma\}$. In our analysis, we incorporated both intra and cross-frequency coupling modes. Adopting our recent Dominant Intrinsic Coupling Mode (DICM) model leads to the construction of an integrated DFCG (iDFCG) that encapsulates both the functional strength but also the DICM of every pair of brain areas. Based on the LO - IDFCG, we constructed the HO- IDFCG by adopting the cosine similarity between the time-series derived from the LO-DIFCG. At a second level, we estimated the laplacian transformations of both LO and HO-IDFCG and by calculating the temporal evolution of Synchronizability (Syn), four network metric time series ($NMTS^{Syn}$) were produced. Following, a machine learning approach based on multi-kernel SVM with the four $NMTS^{Syn}$ used as potential features and appropriate kernels, we succeeded a superior classification accuracy (~98%). DICM and flexibility index (FI) achieved a classification with absolute performance (100 %)

Schizophrenic subjects demonstrated a hypo-synchronization compared to healthy control group which can be interpreted as a low global synchronization of co-fluctuate functional patterns. Our analytic pathway could be helpful both for the design of reliable biomarkers and also for evaluating non-intervention treatments tailored to schizophrenia. EEG offers a low-cost environment for applied neuroscience and the transfer of research knowledge from neuroimaging labs to daily clinical practice.

Keywords: EEG, dynamic functional connectivity graphs, multiplexity, chronnectomics, dominant intrinsic coupling modes, schizophrenia

1. Introduction

Schizophrenia (ScZ) is defined as a brain disconnectivity disorder (Schmitt et al, 2011 ; Friston,1996) characterized by an aberrant fronto-parietal interactions compared to healthy controls (Friston and Frith, 1995). Animal models proved that lesions in the hippocampus may introduce a disconnected pattern in the prefrontal cortex (Schmitt et al, 2011). Magnetic resonance imaging (MRI) studies tailored to schizophrenic patients revealed deficits of gray matter in medial temporal lobe (and hippocampus), in the prefrontal, anterior cingulate, parietal and superior temporal cortex and the thalamus and a magnification of the ventricles (Shenton et al., 2001). Diffusion tensor imaging (DTI) studies have demonstrated a decrement of white matter anisotropy in the temporal and left prefrontal cortex (Kubicki et al., 2007). It is important to underline current evidences that limbic pathways connecting thalamus, anterior cingulate cortex, prefrontal cortex and the hippocampus are activated in information processing and high cognition (Gaebel,2011). A first clinical picture of the aberrant connectivity in schizophrenia may be the decreased of functional integration resulting in the malfunction of association process.

Cortical disconnectivity theory for schizophrenia has been explored also in functional neuroimaging. The analysis of multichannel electro (EEG) and magneto-encephalography (MEG) signals provides unique information for functional interaction between neural oscillations characterizing brain activity of specific areas within the same frequency (intra-frequency coupling) and between frequencies (cross-frequency coupling ; Dimitriadis et al., 2017b,2018c) in high temporal resolution (Canolty and Knight, 2010 ; von Stein and Sarnthein, 2000 ; Lisman and Buzsaki, 2008 ; Dimitriadis et al., 2017b, 2018c). These functional interactions have been proved to be altered in schizophrenia (Allen et al., 2011). The analysis of EEG at resting state condition demonstrated and increased pattern of δ,θ and β activity complementary to a decreased pattern in α frequency within the frontal cortex ("*hypo-frontality*") in schizophrenic patients relative to controls (Ingwar and Franzen, 1974 ; Ragland et al., 2007). An additional potential biomarker for schizophrenia is *abnormal brain asymmetry* (Oertel-Knoechel et al., 2012 ; Gotts et al., 2013 ; Ribolsi et al., 2014 ; Miyata et al., 2012).

A recent EEG study at resting-state explored aberrant functional brain connectivity induced by schizophrenia adopting three connectivity estimators, alternative network metrics and two reference systems (Olejarczyk and Jernajczyk, 2017). They revealed the inter-hemispheric asymmetric group-difference using DTF granger causality estimator at resting-state.

The majority of studies that explored functional connectivity at α frequency band reported a decreased patter in ScZ. In particular, decreased α connectivity estimated by coherence, lagged coherence and phase synchrony, has been reported at frontal (Di Lorenzo, et al., 2015 ; Tauscher et al.,1998), fronto-posterior (Di Lorenzo, et al., 2015, Lehmann et al., 2014) and parieto-temporal (Di Lorenzo, et al., 20150 brain areas (for different results see also Andreou et al., 2015, Kam et al., 2013, Winterer et al., 2011, Merrin and Floyd, 1996). Interestingly, two studies reported a high correlation between functional connectivity at rest in α frequency band with symptoms in ScZ (Hinkley et al., 2011 ; Merrin and Floyd, 1996). Evidences that contradict have been reported in fast oscillations at β (13– 30 Hz) and γ (30–200 Hz) frequencies at rest, including both elevated (Di Lorenzo, et al., 2015), reduced (Kam et al., 2013) and intact (Lehmann et al., 2014, Andreou et al., 2015, Tauscher et al.,1998, Winterer et al., 2011) β frequency band connectivity. Preliminary evidence suggests that β based functional connectivity is influenced by illness progression and clinical symptomatology (Di Lorenzo, et al., 2015). For a systematic review tailored to functional connectivity evidences using EEG in schizophrenia see (Maran et al., 2016).

The majority of studies so far analysed static functional connectivity under the framework of static functional connectivity graphs (FCG) which is constructed by adopting a bivariate or multivariate connectivity estimator that quantifies the signal temporal synchronization across every pair of brain areas. This type of FCG is called low-order (LO) by definition because they characterize EEG signal synchronizations and not high-level inter-regional interactions. A recent study proposed the notion of high-order (HO) FCG by measuring the inter-regional interactions via the similarity between two brain areas' functional topographic profile (Zhang et al., 2017). They demonstrated that HO-FCG complements to LO-FCG in the preliminary design of a novel biomarker tailored to mild cognitive impairment based on resting-state fMRI activity (Zhang et al., 2017).

In the present study, we propose a novel approach by first built an integrated dynamic FCG (IDFCG) by incorporating into a single DFCG both the functional coupling strength and also the dominant intrinsic coupling mode (DICM) between every EEG sensor and also across every temporal segment following a sliding-window approach (Dimitriadis et al., 2017b,2018c). Afterward, we built a subject-specific LO and HO-IDFCG for both the healthy control and schizophrenic group. Every 'quasi-static' snapshot of the LO and HO-IDFCG has been topologically filtered with orthogonal minimal spanning trees algorithm that we have recently proposed (Dimitriadis et al., 2017a, 2017c). Then, we estimated both the un-normalized (LM) and normalized Laplacian matrix (NLM) for every framework of both LO and HO-IDFCG. Following an eigenanalysis of both Laplacian transformations, we then computed the Synchronizability (syn) of the whole LO and HO-IDFCG across experimental time. This procedure leads to a network metric time series ($NMTS^{syn}$) in the four cases (LO-HO IDFCG (2) x LM –NLM (2)). Adopting a multi-kernel learning with updated kernels tailored to proper time-series distance metrics, complementary features from alternative time-varying FC brain networks constructed at different spatial and temporal scales are fused for the construction of a dynamic connectomic biomarker with a superior diagnostic value for ScZ.

In Materials and Methods section, we described the data acquisition and details of the EEG dataset, the pre-processing steps including the denoizing with ICA. The Results section is devoted to describe the results including classification results and significant changes between conditions. Finally, the Discussion section includes the discussion of the current research results with future extensions.

2. Material and Methods

The subjects were adolescents who had been screened by psychiatrist and divided into a healthy group (n = 39) and a group with symptoms of schizophrenia (n = 45). Both groups included only school boys. The age of the group ranged from 10 years and 8 months to 14 years. The healthy control group included 39 healthy schoolboys aged from 11 years to 13 years and 9 months. The mean age in both groups was 12 years and 3 months. EEG activity was recorded from 16 EEG channels at resting-state with eyes-closed. The electrode positions are demonstrated in Figure 1. The sampling rate is 128 Hz and the recording time was 1 min,

thus a total of 7,680 samples refer to 1 min of EEG record. You can download the EEG recordings from the website: http://brain.bio.msu.ru/eeg_schizophrenia.htm .

2.1 Artifact Reduction with Independent Component Analysis (ICA)

Ongoing activity from each modality was corrected for artefacts through the following procedure. Line noise was removed with a notch filter at 60 Hz and the data recording from a single subject was whitened and further reduced in dimensionality by means of Principal Component Analysis (PCA) with a threshold corresponding to 95% of total variance (Delorme and Makeig, 2004). The resulting signals were further submitted to ICA using the extended Infomax algorithm as implemented in EEGLAB (Delorme and Makeig, 2004). A given independent component (IC) was considered to reflect ocular, muscle or cardiac artefacts if more than 30% of its z score kurtosis or skewness values, respectively, were outside ±2 of the distribution mean complementary to the time-course and the spatial distribution of the IC-based weights (Dimitriadis et al., 2015). Finally, the artifactual ICs were zeroed and the artefact free activity was back projected to the original dimension space. Fig.1 illustrates the topology of the EEG sensors.

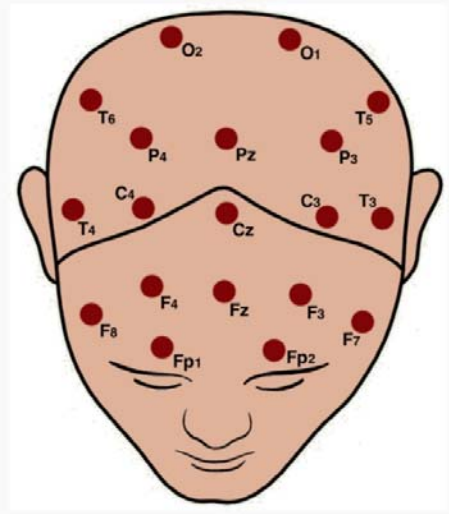

Fig.1 Topology of EEG recording sensors.

2.2 Dynamic iPLV estimates: the dynamic integrated functional connectivity graph based on iPLV (DIFCG^{iPLV} graph)

Here, we describe our dominant intrinsic coupling model (DICM) presented in the majority of functional neuroimaging modalities (Dimitriadis,2018c). The goal of the DICM

model is to uncover the dominant coupling mode between every pair of EEG sensors here and across temporal segments. DICM model explores the dominant coupling mode across intra-frequency coupling and inter-frequency coupling modes based on phase-to-phase and phase-to-amplitude couplings, correspondingly.

We studied dynamic functional connectivity across experimental time and the 16 EEG sensors within and between the seven studying frequency bands {δ, θ, α_1, α_2, β_1, β_2, γ} defined, respectively, within the ranges {0.5–4 Hz; 4–8 Hz; 8–10 Hz; 10–13 Hz; 13–20 Hz; 20–30 Hz; 30–48 Hz}. EEG recordings were bandpass filtered with a 3rd order zero□phase Butterworth filter using filtfilt.m MATLAB function.

The width of the temporal window moved forward across experimental time was set equal to 250ms (or 32 samples), as an adequate number to capture the dynamics of every brain rhythm (fast and slows, Dimitriadis et al.,2013a,b,2015a,b,2016a,b,c,2017a,b,2018b,c). The centre of the temporal window moved forward every 50 ms (6 samples) and both intra and inter□frequency interactions between every possible pair of frequencies were re□estimated leading to a 'quasi□stable' in time static iPLV-based FCG. This approach leads to 1196 temporal segments.

In this manner, a series of iPLV-based graph estimates were computed per subject, for each of the 7 possible intra□frequency coupling refers to the studying frequencies and the 21 possible cross□frequency pairs. This procedure which is described in detail in our previous papers (Dimitriadis and Salis, 2017b ; Dimitriadis et al., 2018c), resulted in 7 $DFCG^{iPLV}$ per participant for within frequency bands and 21 $DFCG^{Iplv}$ per participant for each possible cross□frequency pair. $DFCG^{iPLV}$ tabulates iPLV estimates between every possible pair of sensors. For each subject, a 4D tensor [frequencies bands (28 × temporal segments × sensors x sources] was created for each subject integrating spatiotemporal phase-based interactions. Afterward, we applied surrogate analysis in order to reveal the dominant type of interaction for each pair of sensors and at each snapshot of the DFCG. We constructed 1.000 surrogate time□series by cutting first at a single point at a random location around the middle of the original time series (between 25 s and 35 s), creating two temporal segments and then exchanging the two resulting temporal segments (Dimitriadis and Salis, 2017b ; Dimitriadis et al., 2018c).

The adopted surrogate scheme was applied to the original whole time series and used at every signal□segment at every temporal window. This procedure preserves phase dynamics and the non-stationarity of EEG brain time -series (see Dimitriadis and Salis, 2017b,Dimitriadis,2018c).

Finally, for each pair of sensors and for each temporal segment, we estimated 1.000 iPLV for every within frequency interaction and every possible pair of frequencies. Practically, we assigned a p□value to each within and between frequencies interaction and for each sensors/sources/ROIs by comparing the original iPLV value with 1.000 surrogates $iPLV^{Surr}$, we corrected for multiple comparisons across 28 possible DICM in order to reveal a DICM per pair of EEG sensors and for each temporal segment. There are in total three scenarios:

1. a no p□value survived the multiple correction ($p' < p/28$)

where $p = 0.05$)

2. more than one survived and in that case, we selected the DICM

with the maximum iPLV/WC value or

3. only one survived the multiple correction

Figure 2a illustrates how the DICM is defined in the first two temporal segments from the EEG dataset between F7 and F3 EEG sensors. Finally, we tabulated both the strength and the type of dominant coupling mode in 2 3D tensor [1196 x 16 x 16], one that keeps the strength of the coupling based on iPLV and a second one for keeping the dominant coupling of interaction using integers from 1 up to 28:1 for δ, 2 for θ, …, 7 for γ, 8 for $\delta - \theta$, …, 28 for $\beta_2 - \gamma$}. The notion of phase□to□amplitude cross□frequency coupling (CFC) estimator has been employed also in our previous studies with EEG/MEG brain datasets (Dimitriadis and Salis, 2017b, Dimitriadis et al., 2017c,2018a,b,c,d). Figure 2b demonstrates the temporal evolution of DICM across experimental time for F7-F3 EEG pair while the comodulogram on the right side tabulates the PD of the DICM for this semantic time series.

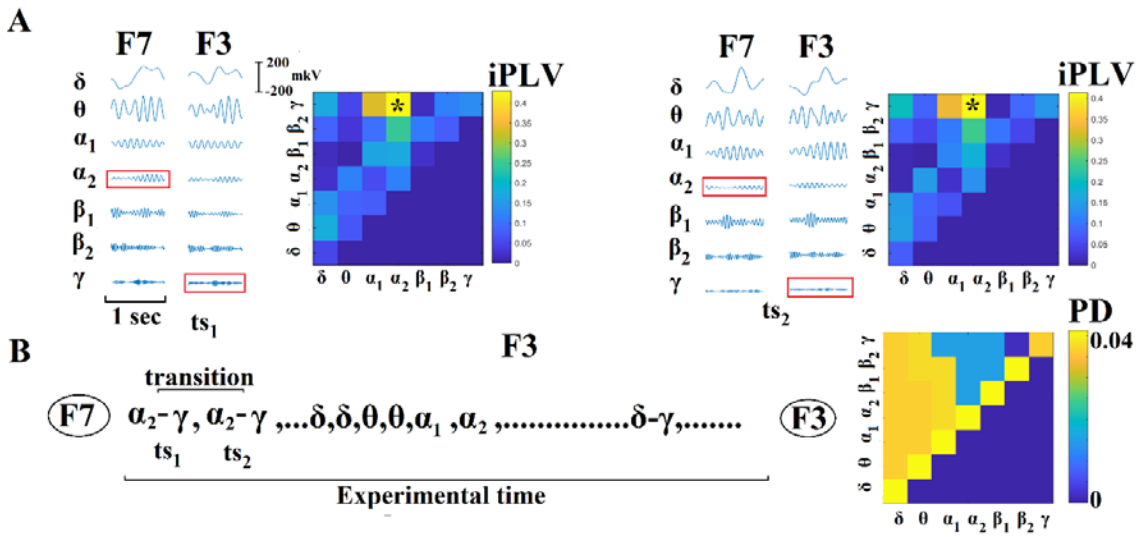

Figure 2. Determining Dominant Intrinsic Coupling Modes (DICM).
(a) Schematic illustration of the approach employed to identify the DICM between two EEG sensors (F3 and F7) for two consecutive temporal segment (ts_1, ts_2) during the resting state EEG activity from the first normal subject. In this example the functional interdependence between band passed signals from the two sensors was indexed by imaginary Phase Locking (iPLV). In this manner iPLV was computed between the two EEG sensors either at same frequency oscillations (e.g., δ to δ) or between different frequencies (e.g., δ to θ). Statistical filtering, using surrogate data approach was employed to assess whether each iPLV value was significantly different than chance. During ts_1 the DICM reflected significant phase locking between α_2 and γ oscillations (indicated by red rectangles) while during in ts_2 the dominant interaction was remain stable.
(b) Burst of DICM between the two sensors. This packeting can be thought to associate the "letters" contained in the DICM series to form a neural "word.", a possible integration of many DICM (Buzsaki & Watscon, 2012). For the first pair of ts_{1-2}, we illustrated the statibility of DICM for the first pair and a transition between δ - θ and θ- α_1 is defined for F7 F3 EEG pair important for the estimation of FI (see section 2.3). The comodulogram on the right demonstrates the probability distribution (PD) of the DICM across temporal segments for the EEG sensor pair F7-F3.

2.3 Semantic Features Derived from the evolution of DICM

This section describes the semantic features that can be defined by analysing the 2nd 3D tensor that preserves the DICM across spatio-temporal space.

2.3.1 Flexibility Index (FI)

Based on the 2nd 3D tensor DIFCG that keeps the information of the DICM per pair of sensors and across time, we estimated the transition rate for every possible pair of sensors. The previous defined estimator was called flexibility index (FI) and quantifies how many times every pair of sensors changes DICM across experimental time (Dimitriadis and Salis,2017b ; Dimitriadis,2018c). This metric will called hereafter FI^{DICM} which is defined as:

$$FI^{DICM} = \frac{no\ of\ transitions}{temporal\ segments - 1} \quad (1)$$

FI^{DICM} gets higher values for higher "jumps" of DICM between a pair of EEG sensors across experimental time. Figure 2b illustrates how FI^{DICM} is estimated for F3-F7 EEG pair. This approach leads to a sensor x sensor (16 x 16) matrix per subject or $16^2 - 16 = 140$ FI features.

2.3.2 Spatiotemporal distribution of DICM— comodulograms

Based on the 2nd 3D DIFCG that keeps the semantic information of the preferred dominant coupling mode, we can tabulate in a frequencies × frequencies matrix the probability distribution (PD) of observing each of the DICM frequencies across 7 (intra-frequency) + 21 (cross-frequency coupling) = 28 possible coupling modes and exploring their spatio-temporal distribution.

The spatiotemporal PD tabulated in a matrix is called hereafter comodulogram and an example is demonstrated in Fig.2b (Antonakakis et al., 2016,2017a,b ; Dimitriadis and Salis,2017b,c ; Dimitriadis,2018a,c,d). PD is a new vector of features with dimension 1 x 21 possible DICM.

2.4 Low and High-order DFCG

In section 2.2, we described the construction of DIFCG also called as low-order DIFCG (LO-DIFCG). Here, we will define the construction of the high-order DIFCG (HO-DIFCG). The HO-DFCG was constructed by estimating the 'cosine' similarity between every pair of the time-series that each one describes the fluctuation of functional strength of a pair of EEG sensors. Here, we quantified the cosine similarity of the fluctuations of iPLV by

taking into consideration a temporal window of 10 temporal segments sampled from the LO-DIFCG with moving step equals to 1. This means that the 1st temporal dimension of the HO-DFCG is equal to 1187. A LO-FCG has dimensions of 16 x16 while a HO-FCG has dimensions 240 x 240. LO-DIFCG has dimensions of 1196 x 16 x16 while HO-DIFCG has dimensions of 1187 x 240 x 240. Afterward, we topologically filtered both LO and HO-FCG with our OMST method at every temporal segment (Dimitriadis et al., 2017a,c).

Practically, HO-DIFCG captures the level of co-fluctuation of functional coupling across EEG-pairs across experimental time. A high cosine similarity value between two pairs of EEG-pairs is interpreted as a high temporal co-fluctuation behaviour.

Fig.3a illustrates the first 20 temporal segments of the LO-DIFCG starting with a full-weighted FCG, a statistical filtering version of FCG and its normalized laplacian transformation (see next section). Similarly, in Fg.3b, we illustrated the first 20 temporal segments of the HO-DIFCG and its pre-processing steps.

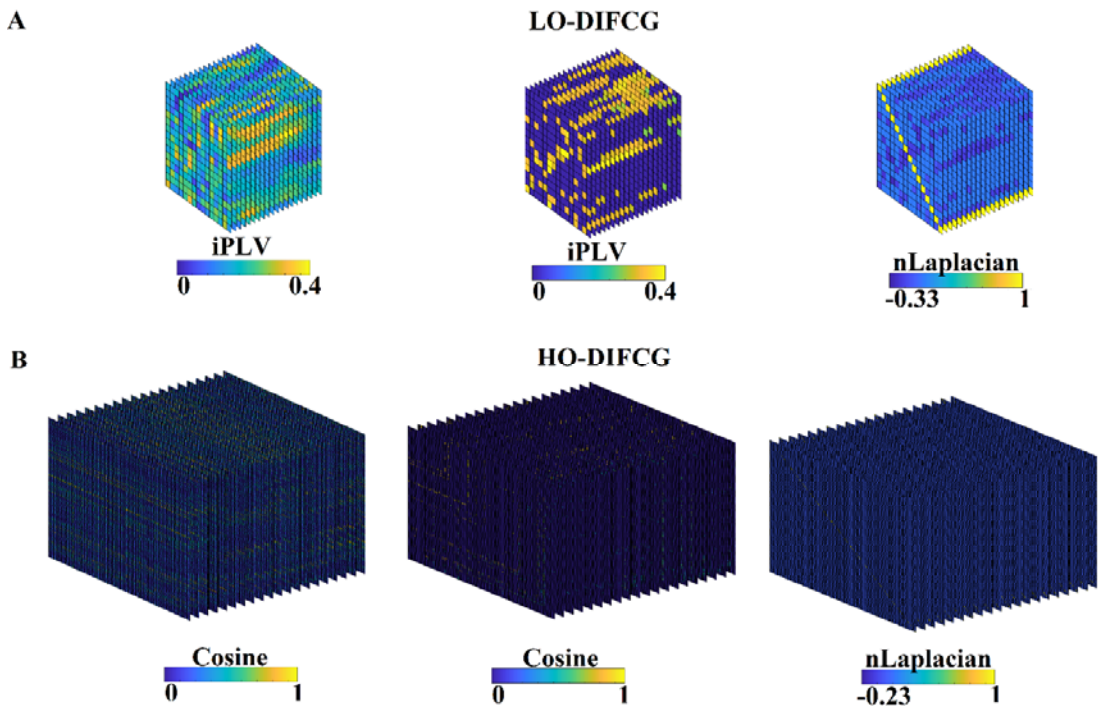

Figure 3. Pre-processing steps of a) LO and b) HO-DIFCG.

First column demonstrates the full-weighted LO and HO-DIFCG, the second column illustrates the statistically and topologically filtered versions while the third column refers to their normalized laplacian transformations.

2.5 Graph Signal Processing of LO and HO-DFCG : Evolving Synchronizability

Given a simple graph FC*G* with *n* vertices, its Laplacian matrix L is defined as (Chung,1997):

L = D – A (2)

where *D* is the degree matrix and *A* is the adjacency matrix of the graph. Since FCG is a weighted graph, A only contains weights related to the functional strength and its diagonal elements are all 0s.

In the case of directed graphs, either the in-degree or out-degree might be used, depending on the application. Here, we employed the degree for LO and the in-degree for HO-DIFCG.

The elements of L are given by

$$L_{i,j} = \begin{Bmatrix} degree\ or\ in-degree(u_i) & if\ i=j \\ -FCG(i,j)\ if\ i \neq j\ and\ u_i\ is\ adjacent\ to\ u_j & \\ 0 & otherwise \end{Bmatrix} \quad (3)$$

where deg(v_i) is the degree of the vertex i.

The symmetric normalized Laplacian matrix is defined as:

$$nL = D^{-\frac{1}{2}} L D^{-\frac{1}{2}} = I - D^{-\frac{1}{2}} A D^{-\frac{1}{2}} \quad (4)$$

The elements of NL are given by:

$$nL_{i,j} = \begin{Bmatrix} degree\ or\ in-degree(u_i) & if\ i=j\ and\ in\ \mathrm{degree}(u_i) \\ -\dfrac{1}{\sqrt{\mathrm{degree\ or\ in_degree}(u_i)\, x\ degree\ or\ in\ _\mathrm{degree}(u_j)}}\, x\ FCG(i,j) & if\ i \neq j\ and\ u_i\ is\ adjacent\ to\ u_j \\ 0 & otherwise \end{Bmatrix}$$

We estimated both L and NL for every snapshot of LO and HO-DIFCG. Then, we calculated the eigenratio of the L and NL matrix of every quasi-static FCG, i.e., the largest eigenvalue divided by the second smallest one which is called Synchronizability (Syn). The whole analysis produces 2 x 2 network metric time series ($NMTS^{Syn}$) per subject related to {LO and HO-DIFCG} x {L and NL}. Fig.4 demonstrates the four $NMTS^{Syn}$ from the first HC and ScZ subjects.

2.5 Signal Power Analysis

We estimated the relative power spectrum (RSP) of every EEG sensor and frequency band in both groups. Welch's algorithm was adopted using MATLAB function pwelch leading to the estimation of power spectrum per frequency band first and then their percentage across total power spectrum leading to RSP. Group statistical analysis across sensors and frequency bands have been performed with Wilcoxon Rank Sum test ($p < 0.05$, Bonferroni corrected, $p' < p/(16*7)$ where 16 refers to EEG sensors and 7 to the number of the studying frequency bands).

2.7 Multi-kernel SVM Classification

We divided the whole analysis of corrected classifying ScZ subjects from HC in two parts. The first analysis focused on the analysis of PD of DICM (comodulograms) and FI derived by the DIFCG that keeps the semantic information of the DIFCG, the dominant intrinsic coupling modes. The second analysis focused on the four $NMTS^{Syn}$ derived from LO and HO-DIFCG and eigenanalysis of L and NL.

We hypothesized that PD and FI and the four $NMTS^{Syn}$ provide complementary information to each other. To improve potential classification performance, we decided to fuse those features to further improve the classification performance. Vectorizing the features is not an optimal approach while $NMTS^{Syn}$ should be treated as time series. A kernel-based feature combination using multi-.kernel learning offers an alternative approach by weighting differently evert feature derived from a different but complementary procedure (Jie et al., 2015). Such an approach may provide a better way to integrate the features derived from different approaches and types of DIFCG networks.

We adopt a multi-kernel learning to fuse the features by a linear combination of kernels that are estimated from the PD (21 features) and FI (240 features) and by LO and HO-DIFCG, the four $NMTS^{Syn}$. An SVM classifier with a linear kernel $K(\mathbf{a}, \mathbf{b}) = \mathbf{a}^T \mathbf{b}$ based on LIBSVM (Chang and Lin,2011) was employed for the multi-kernel learning based classification based on PD and FI features. The features were first normalized to make sure that all the features are comparable. A linear kernel is calculated across subjects separately for PD and FI. A composite kernel through an optimal linear combination of the multiple kernels was adopted as an optimal fusion of the features. We classified every subject with SVM with the composite kernel following a 10-fold cross-validation (CV) scheme 100 times.

Specifically, for the semantic approach using PD and FI, we followed a 10-fold CV using the 90% for feature selection following a 5-fold CV for feature selection and ranking across the 100 runs x 5 (CV)= 500 times. As a feature selection algorithm, we adopted infinite feature selection algorithm (Roffo et al., 2015). Feature selection has been aaplied within every fold of the 5 CV and across runs. From the ranking of 261 features (21 : PD + 240 : FI), we kept the first 30 ranked features.

Particularly for the four $NMTS^{Syn}$, we adopted as a proper kernel tailored to $NMTS^{Syn}$ based on dynamic time wrapping which is a proper distance metric between the $NMTS^{Syn}$ and also Kullback-Leibder divergence histogram distance metric.

Fig.4 illustrates representatives $NMTS^{Syn}$ from the first subject of each group extracted from both LO and HO-DIFCG and also from both L and NL transformations.

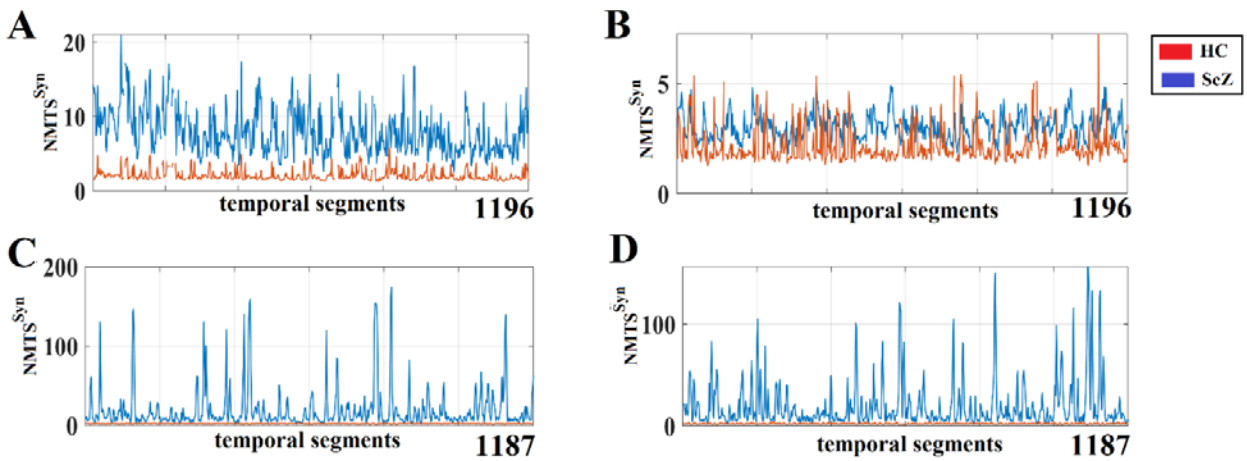

Fig.4. Illustration of representative $NMTS^{Syn}$ from both groups in the four cases.

- **a)** Laplacian transformation derived from LO-DIFCG
- **b)** Normalized Laplacian transformation derived from LO-DIFCG
- **c)** Laplacian transformation derived from HO-DIFCG
- **d)** Normalized Laplacian transformation derived from HO-DIFCG

3.Results

3.1 Contribution of $NMTS^{Syn}$ to High Classification Performance of Sch Subjects

Tables 1 summarizes the evaluation of classification performance based on the four $NMTS^{Syn}$, dynamic time wrapping metric and Kullback-Leibder divergence histogram distance metric in the four possible pairs of combinations. The highest accuracy succeeded in

LO-DIFCG by combining both L and NL transformations and also by combing the laplacian transformation of LO and HO-DIFCG.

Similarly, Tables 2 summarizes the evaluation of classification performance based on the four $NMTS^{Syn}$ and the Kullback-Leibder divergence histogram distance metric in the four possible pairs of combinations. The highest accuracy succeeded in three out of four combinations with the exception of the normalized laplacian transformation of LO and HO-DIFCG (Table 2).

Table 1. Evaluation of Classification performance based on $NMTS^{Syn}$, dynamic time wrapping and a multiple-kernel SVM approach.

	Accuracy	**Sensitivity**	**Specificity**
LO-DIFCG (L+NL)	0.98 ± 0.0052	0.97 ± 0.0052	1.00 ± 0.00
HO-DIFCG (L+NL)	0.90 ± 0.02	0.95 ± 0.02	0.96 ± 0.03
HO and LO-DIFCG (L)	0.98 ± 0.052	0.97 ± 0.052	0.98 ± 0.01
HO and LO-DIFCG (NL)	0.90 ± 0.02	0.95 ± 0.01	0.96 ± 0.01

Table 2. Evaluation of Classification performance based on $NMTS^{Syn}$, Kullback-Leibder divergence histogram distance metric and a multiple-kernel SVM approach.

	Accuracy	**Sensitivity**	**Specificity**
LO-DIFCG (L+NL)	0.97 ± 0.0052	0.96 ± 0.01	0.97 ± 0.01
HO-DIFCG (L+NL)	0.98 ± 0.01	0.97 ± 0.01	0.96 ± 0.01
HO and LO-DIFCG (L)	0.98 ± 0.052	0.97 ± 0.052	0.98 ± 0.01
HO and LO-	0.87 ± 0.03	0.90 ± 0.02	0.92 ± 0.02

DIFCG (NL)			

3.2 Contribution of Semantic Features based on DICM model for High Classification Performance of Sch Subjects

Our machine learning strategy revealed 15 consistent features among FI and PD of DICM. Fig.5 (a-d) illustrates the spatial distribution of the FI across every possible pair of EEG sensors

for HC and ScZ group, correspondingly. Feature selection strategy revealed 10 FI features that are located over fronto–temporo–parietal network and denoted with '*'. Figure 6 (e-f) illustrates the group□averaged comodulograms for HC and ScZ group, correspondingly. Five more features were selected that referred to the PD across space and time of δ□θ, δ□α_1, δ□α_2, δ□β_1 and θ□α_1 intrinsic coupling modes. ScZ patients demonstrated lower PD values compared to HC. The classification performance based on selected FI+PD features was absolute (100%). Table 3 tabulates the performance for each set of features and also their integration.

Finally, Fig.5(f) demonstrates the Score of the selected features across 100 runs x 5 – fold CV which refers to the number of times a feature is selected as informative to discriminate HC from ScZ group.

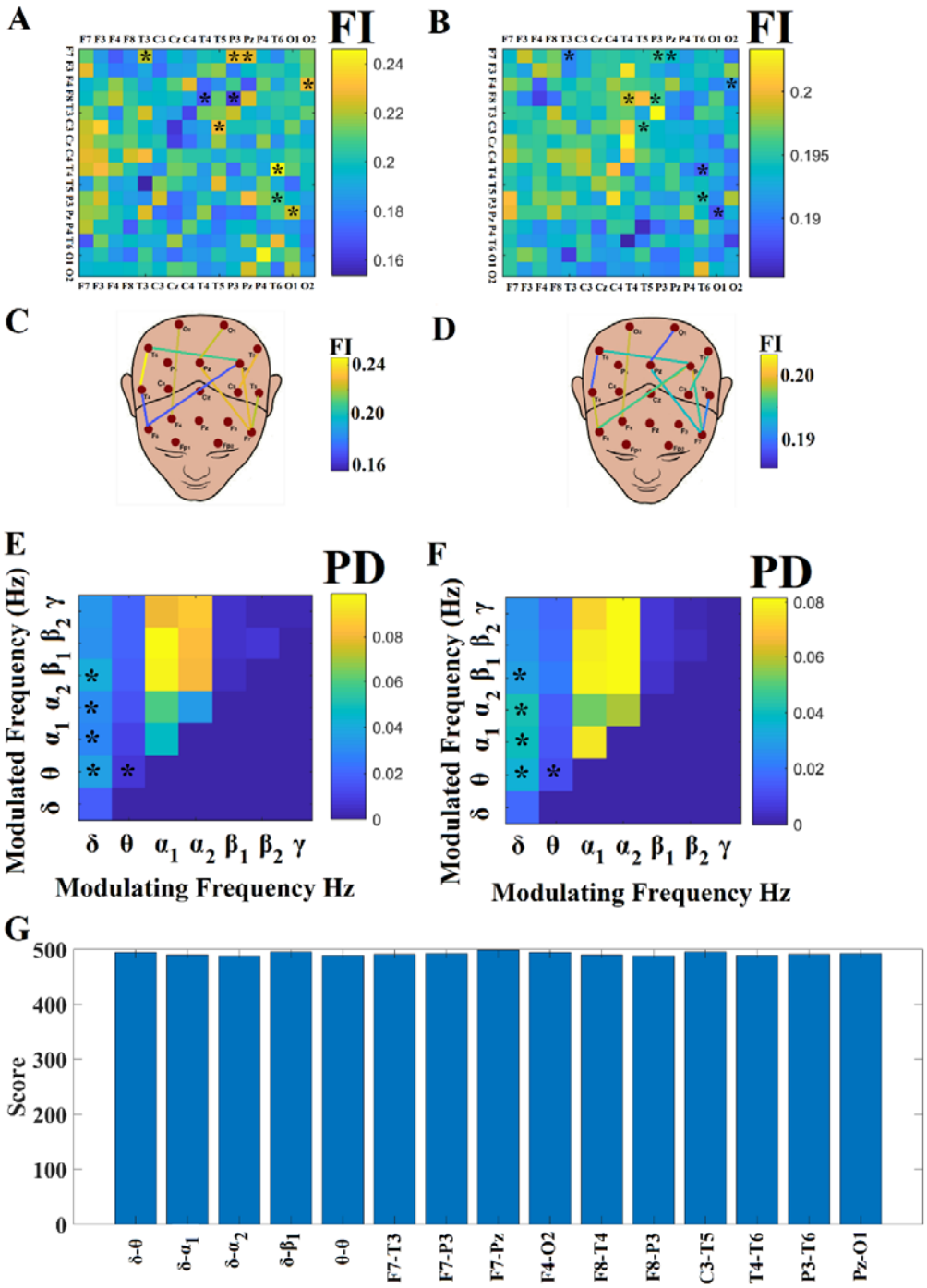

Fig.5 Group□Averaged Flexibility Index (FI) and Comodulograms that tabulate the PD of spatio-temporally DICM.
(a,b) Group□averaged FI for healthy control (HC) (a) and schizophrenic (ScH) group (b).
(c, d) Group□averaged comodulograms for HC
(c) and ScZ group
(d) probability distribution of DICM across space and time averaged across subjects in
(e) HC group and in (f) ScZ group.
(g) Total score of the selected features demonstrated in a – f across 100 runs x 5-fold CV = 500 times.

Every FI and PD has been selected via the feature selection algorithm is denoted with '*'.

Table 3. Evaluation of Classification performance based the semantic features pool of PD and FI and on a multiple-kernel SVM approach.

	Accuracy	**Sensitivity**	**Specificity**
PD	1.00 0.00	1.00 0.00	1.00 0.00
FI	1.00 0.00	1.00 0.00	1.00 0.00
PD+FI	1.00 0.00	1.00 0.00	1.00 0.00

3.3 Relative Signal Power in HC and ScZ subjects

Statistical analysis of RSP between the two groups across EEG sensor space and frequency bands revealed significant higher δ RSP for ScZ compared to HC in O1 and O2 EEG sensors. Fig.6 illustrates a global tendency (no statistical significant) of higher RSP values in δ and θ frequencies in ScZ compared to HC subjects.

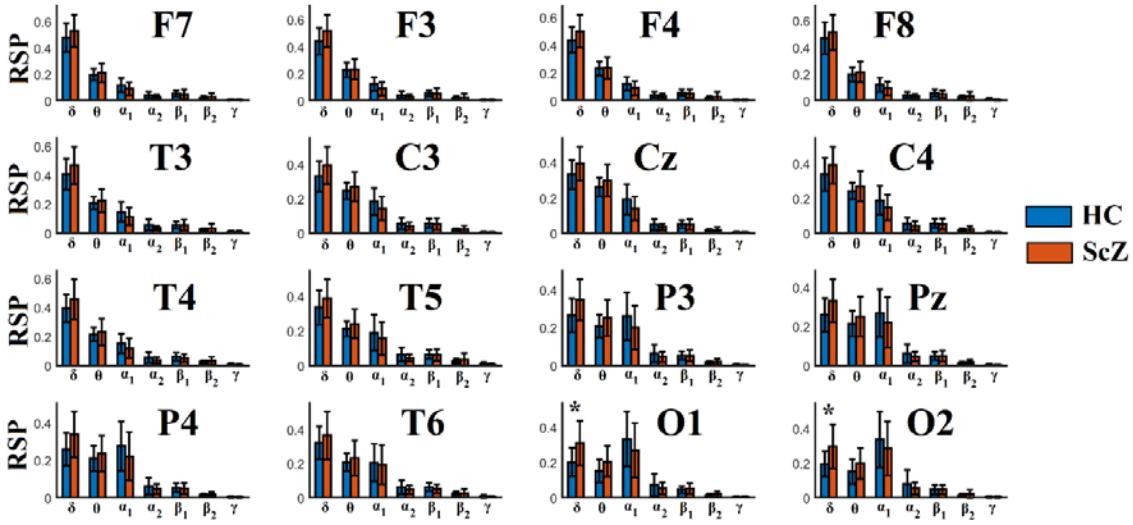

Figure 6. Relative Signal Power (RSP) across EEG sensor space and frequency bands in HC and ScZ patients.

Our analysis revealed significant higher δ RSP for ScZ compared to HC in O1 and O2 EEG sensors.

(* Wilcoxon Rank Sum test ($p < 0.01$, Bonferroni corrected, $p' < p/(16*7)$ where 16 refers to EEG sensors and 7 to the number of the studying frequency bands).

4.Discussion

In the present study, we investigated the contribution of graph signal processing over LO and HO-DIFCG and semantic information derived from our DICM model to the diagnosis of schizophrenia. Following a data-driven model from EEG recordings up to the set of novel chronnectomics metrics, we succeeded to discriminate HC from ScZ patients with absolute accuracy. Laplacian transformations of LO and HO-DIFCG gives the baton to the estimation of the Synchronizability giving rise to four representative $NMTS^{Syn}$ per subject. DICM model extracts 261 features explicitly refer to PD (21 features) and FI (240 features) per subject. Following an integrated multi-kernel learning SVM approach, we succeeded to discriminate ScZ patients from HC with 98% using $NMTS^{Syn}$ and 100% employing PD and FI.

It is important to draw attention to neuroscientists working on functional neuroimaging the significance of exploring simultaneously the spatio-temporal behaviour of functional strength complementary to the PD of DICM across space and time. Here, we revealed a global temporal hypo-synchronization of ScZ patients compared to HC subjects (Fig.4). This hypo-synchronization in HO-DIFCG can be interpreted as a loss of co-fluctuation property of dynamic functional coupling between pairs of EEG pairs.

Complementary, our analysis revealed a less flexible brain for ScZ patients which is interpreted as less switching functional interactions between dominant intrinsic coupling modes. The spatial distribution of the FI features is extended between EEG sensors located over fronto–temporo–parietal brain areas. Feature selection strategy revealed lower PD values for ScZ patients for five intrinsic coupling modes : $\delta\square\theta$, $\delta\square\alpha_1$, $\delta\square\alpha_2$, $\delta\square\beta_1$ and $\theta\square\alpha_1$ (Fig.5).

Schizophrenia includes an abnormal functionality of many brain areas including the hippocampus (Tamminga et al.,2010). Hippocampal changes explained memory abnormalities observed in schizophrenia and may affect also other brain areas. Specifically, in ScZ patients, researchers observed an hyper-activity of CA1 (Lodge and Grace,2011). *N*-methyl-D-aspartate receptor (NMDAR) antagonist mimicked many symptoms of schizophrenia (Zhang et al., 2012). Of great importance is the enhancement of δ activity at awake state in schizophrenia, an aberrant functionality that can be explained by NMDAR antagonist action in the thalamus that can stimulate thalamic activity and produce δ oscillations (Sharp and Hendren 2007). Here, we detected significant higher RSP in δ frequency in ScZ patients compared to HC in O1 and O2 EEG sensors (Fig.6).

Many previous studies explored the contribution of both low and high frequency oscillations to explain a range of cognitive deficits in schizophrenia modulated with specific frequency content (Moran and Hong,2011). A large study explored the hierarchical organization of γ and θ oscillations in schizophrenia during a 40 Hz auditory steady-state stimulation. They found out that ScZ patients revealed a reduced γ inter-trial phase coherence, increased θ amplitude, and normal θ-phase γ-amplitude cross-frequency coupling (Kirihara et al., 2012).

It is important to state here that this is the very first study that explored simultaneously both intra-frequency and cross-frequency interactions in Schizophrenia under DICM model. Under this framework, we can decipher the multiplexity of complex electrophysiological aberrant connectivity observed in schizophrenic patients by integrating the available intrinsic coupling modes.

Our DICM model untangled the multiplex syntactic rules which are important for the exchange of information across the cortex (Buzsaki & Watscon, 2012). DICM model hypothesizes that the dynamic reconfiguration of dominant intrinsic coupling modes can capture the multiplexity and complexity of functional brain connectivity during both spontaneous and cognitive tasks. Additionally, the flexibility of this reconfiguration can be linked to the multiplexity of brain functionality and can be estimated via FI. FI can be seen as a reflex index that describes the readiness of the brain to respond to new stimuli.

It would be interesting to follow the same methodology during cognitive tasks and also on the source level in order to get the advantage of animal models and fMRI studies that revealed the mechanistic explanation of aberrant networks in schizophrenia (Hunt et al., 2017).

5.Limitations

The whole study is unique, innovative and pioneering in terms of analytic pathway and scientific results. However, there are two basic limitations. The first refers to the interpretation of the results on the EEG surface level instead of virtual cortical sources. It would be interesting to follow the same methodological approach in an EEG study recorded healthy controls and schizophrenic patients using a large number of EEG net sensors that support the source reconstruction approach. The second drawback is the limitation of the adopted free database to EEG recordings only without any access to neuropsychological assessment battery. This missing part prevented us to correlate the novel chronnectomic and semantic features with trivial neuropsychological estimates.

Acknowledgments

SD was supported by MRC grant MR/K004360/1 (Behavioral and Neurophysiological Effects of Schizophrenia Risk Genes: A Multi-locus, Pathway Based Approach). SD is also supported by a MARIE-CURIE COFUND EU-UK Research Fellowship. We would like to acknowledge RCUK of Cardiff University and Wellcome Trust for covering the publication fee.

References

Allen EA, Lin J, Kiehl KA, Gelernter J, Pearlson GD, Perrone-Bizzozero NI, Calhoun VD. Components of cross-frequency modulation in health and disease. Front Syst Neurosci. 2011; 5:59 doi: 10.3389/fnsys.2011.00059

Andreou C, Leicht G, Nolte G, Polomac N, Moritz S, Karow A, et al. Resting-state theta-band connectivity and verbal memory in schizophrenia and in the high-risk state. Schizophr Res. 2015;161(2–3):299–307.

Antonakakis, M., Dimitriadis, S. I., Zervakis, M., Micheloyannis, S., Rezaie, R., Babajani□Feremi, A., … Papanicolaou, A. C. (2016). Altered crossfrequency coupling in resting□state MEG after mild traumatic brain injury. *International Journal of Psychophysiology*, *102*, 1–11. https:// doi.org/10.1016/j.ijpsycho.2016.02.002

Antonakakis, M., Dimitriadis, S. I., Zervakis, M., Papanicolaou, A. C., & Zouridakis, G. (2017a). Reconfiguration of dominant coupling modes in mild traumatic brain injury mediated by δ□band activity: A resting state MEG study. *Neuroscience*, *25*(356), 275–286. Epub 2017 May 31. https://doi.org/10.1016/j.neuroscience.2017.05.032

Antonakakis, M., Dimitriadis, S. I., Zervakis, M., Papanicolaou, A. C., & Zouridakis, G. (2017b). Altered rich□club and frequency□dependent subnetwork organization in mild traumatic brain injury: A MEG resting□ state study. *Frontiers in Human Neuroscience*, *11*, 416. eCollection. https://doi.org/10.3389/fnhum.2017.00416

Buzsáki, G., & Watson, B. O. (2012). Brain rhythms and neural syntax: Implications for efficient coding of cognitive content and neuropsychiatric disease. *Dialogues in Clinical Neuroscience*, *14*(4), 345–367.

Canolty RT, Knight RT. The functional role of cross-frequency coupling. Trends Cogn. Sci. 2010; 14(11): 506–515. doi: 10.1016/j.tics.2010.09.001

Chang, C.-C. & Lin, C.-J. Libsvm: a library for support vector machines. *ACM Transactions on Intelligent Systems and Technology* 2, 1–27 (2011).

Chen, Y.□H., Stone□Howell, B., Edgar, J. C., Huang, M., Wootton, C., Hunter, M. A., … Cañive, J. M. (2016). Frontal slow□wave activity as a predictor of negative symptoms, cognition and functional capacity in schizophrenia. *British Journal of Psychiatry*, *208*(02), 160–167. Epub 2015 July 23. https://doi.org/10.1192/bjp.bp.114.156075

Chung, Fan (1997) . *Spectral Graph Theory*. American Mathematical Society.

Delorme, A., & Makeig, S. (2004). EEGLAB: An open source toolbox for analysis of single□trial EEG dynamics including independent component analysis. *Journal of Neuroscience Methods*, *134*, 9–21. https://doi.org/10.1016/j.jneumeth.2003.10.009

Di Lorenzo G, Daverio A, Ferrentino F, Santarnecchi E, Ciabattini F, Monaco L, et al. Altered resting-state EEG source functional connectivity in schizophrenia: the effect of illness duration. Front Hum Neurosci. 2015;9:234.

Dimitriadis, S. I., Laskaris, N. A., & Tzelepi, A. (2013b). On the quantizationof time□varying phase synchrony patterns into distinct Functional Connectivity Microstates (FCμstates) in a multi□trial visual ERP paradigm. *Brain Topography*, *26*, 397–409. https://doi.org/10.1007/
s10548-013-0276-z

Dimitriadis, S. I., Laskaris, N. A., Simos, P. G., Micheloyannis, S., Fletcher,J. M., Rezaie, R., & Papanicolaou, A. C. (2013b). Altered temporal correlations in resting□state connectivity fluctuations in children with reading difficulties detected via MEG. *Neuroimage*, *83*, 307–317.https://doi.org/10.1016/j.neuroimage.2013.06.036

Dimitriadis, S. I., Laskaris, N. A., Bitzidou, M. P., Tarnanas, I., & Tsolaki,M. (2015a). A novel biomarker of amnestic MCI based on dynamic cross□frequency coupling patterns during cognitive brain responses.*Frontiers in Neuroscience*, *9*, 350. https://doi.org/10.3389/ .2015.00350

Dimitriadis, S. I., Laskaris, N. A., & Micheloyannis, S. (2015b). Transition dynamics of EEG□based network microstates unmask developmental and task differences during mental arithmetic and resting wakefulness. *Cognitive Neurodynamics*, *9*, 371–387. https://doi.org/10.1007/s11571-015-9330-8

Dimitriadis, S. I., Laskaris, N. A., Simos, P. G., Fletcher, J., & Papanicolaou,A. C. (2016a). Greater repertoire and temporal variability of Cross□Frequency Coupling (CFC) modes in resting□state neuromagnetic recordings among children with reading difficulties. *Frontiers in Human Neuroscience*, *10*, 63. https://doi.org/10.3389/fnhum.2016.00163

Dimitriadis, S. I., Sun, Y., Laskaris, N., Thakor, N., & Bezerianos, A. (2016b).Revealing cross□frequency causal interactions during a mental arithmetic task through symbolic transfer entropy: A novel vectorquantization approach. *IEEE Transactions on Neural Systems and*
Rehabilitation Engineering, *24*(10), 1017–1028.

Dimitriadis, S. I., Tarnanas, I., Wiederholdg, M., Wiederholdh, B., Tsolaki, M., & Fleische, E. (2016c). Mnemonic strategy training of the elderly at risk for dementia enhances integration of information processing via cross□frequency coupling. *Alzheimer's & Dementia*, *2*, 241–249.https://doi.org/10.1016/j.trci.2016.08.004

Dimitriadis, S. I., Salis, C., Tarnanas, I., and Linden, D. (2017a). Topological filtering of dynamic functional brain networks unfolds informative chronnectomics: a novel data-driven thresholding scheme based on orthogonal minimal spanning trees (OMSTs). *Front. Neuroinform.* 11:28. doi: 10.3389/fninf.2017.00028

Dimitriadis, S. I., and Salis, C. I. (2017b). Mining time-resolved functional brain graphs to an EEG-based chronnectomic brain aged index (CBAI). *Front. Hum. Neurosci.* 11:423. doi: 10.3389/fnhum.2017.00423

Dimitriadis, S. I., Antonakakis, M., Simos, P., Fletcher, J. M., and Papanicolaou, A. (2017c). Data-driven topological filtering based on orthogonal minimal spanning trees: application to multi-group MEG resting-state connectivity. *Brain Connect*. 7, 661–670. doi: 10.1089/brain.2017.0512

Dimitriadis, S. I., López, M. E., Bruña, R., Cuesta, P., Marcos, A., Maestú, F., et al. (2018a). How to build a functional connectomic biomarker for mild cognitive impairment from source reconstructed MEG resting-state activity: the combination of ROI representation and connectivity estimator matters. *Front. Neurosci.* 12:306. doi: 10.3389/fnins.2018.00306

Dimitriadis, S. I., Routley, B., Linden, D. E., & Singh, K. D. (2018b). Reliability of static and dynamic network metrics in the resting state: A MEG beamformed connectivity analysis.

Front. Neurosci., 03 August 201| https://doi.org/10.3389/fnins.2018.00506

Dimitriadis SI (2018c). Complexity of brain activity and connectivity in functional neuroimaging.J Neurosci Res. 2018 Nov;96(11):1741-1757. doi: 10.1002/jnr.24316.

Dimitriadis SI, P. Simos, J. Fletcher, A. (2018d) PapanicolaouAberrant resting-state functional brain networks in dyslexia: symbolic mutual information analysis of neuromagnetic signals .Int. J. Psychophysiol. (February) (2018), pp. 1-22

Friston KJ. Theoretical neurobiology and schizophrenia. Br. Med. Bull 1996; 52(3): 644–55.

Friston KJ, Frith CD. Schizophrenia: a disconnection syndrome? Clin Neurosci 1995; 3: 88–97.

Gaebel W (Ed.). Schizophrenia: Current science and clinical practice. Wiley-Blackwell, 2011.

Gotts SJ, Jo HJ, Wallace GL, Saad ZS, Cox RW, Martin A. Two distinct forms of functional lateralization in the human brain. Proc Natl Acad Sci U S A. 2013; 110(36): E3435–44. doi: 10.1073/pnas.1302581110

Hinkley LB, Vinogradov S, Guggisberg AG, Fisher M, Findlay AM, Nagarajan SS. Clinical symptoms and alpha band resting-state functional connectivity imaging in patients with schizophrenia: implications for novel approaches to treatment. Biol Psychiatry. 2011;70(12):1134–42.

Hunt MJ, N.J. Kopell, R.D. Traub, M.A. WhittingtonAberrant network activity in schizophrenia

Trends Neurosci, 40 (2017), pp. 371-382

Ingwar DH, Franzen G. Abnormalities of cerebral blood flow distribution in patients with chronic schizophrenia. Acta Psychiat. Scand. 1974; 50: 425–462.

Jie, B., Zhang, D., Cheng, B. & Shen, D. Manifold regularized multitask feature learning for multimodality disease classification. *Human Brain Mapping* 36, 489–507 (2015).

Kam JW, Bolbecker AR, O'Donnell BF, Hetrick WP, Brenner CA. Resting state EEG power and coherence abnormalities in bipolar disorder and schizophrenia. J Psychiatr Res. 2013;47(12):1893–901.

Kirihara K, A.J. Rissling, N.R. Swerdlow, D.L. Braff, G.A. Light. Hierarchical organization of gamma and theta oscillatory dynamics in schizophrenia.Biol. Psychiatry, 71 (10) (2012), pp. 873-880

Kubicki M, McCarley R, Westin CF, Park HJ, Maier S, Kikinis R, Jolesz FA, Shenton ME. A review of diffusion tensor imaging studies in schizophrenia. J Psychiatr Res. 2007; 41(1–2): 15–30. doi: 10.1016/j.jpsychires.2005.05.005

Lehmann D, Faber PL, Pascual-Marqui RD, Milz P, Herrmann WM, Koukkou M, et al. Functionally aberrant electrophysiological cortical connectivities in first episode medication-naive schizophrenics from three psychiatry centers. Front Hum Neurosci. 2014;8:635.

Lisman J, and Buzsaki G. A Neural Coding Scheme Formed by the Combined Function of Gamma and Theta Oscillations. Schizophr. Bull. 2008; 34: 974 doi: 10.1093/schbul/sbn060

Lodge DJ, Grace AA. Hippocampal dysregulation of dopamine system function and the pathophysiology of schizophrenia.Trends Pharmacol Sci. 2011 Sep; 32(9):507-13.

Maran M, T. Grent-t-Jong, P.J. UhlhaasElectrophysiological insights into connectivity anomalies in schizophrenia: a systematic review. Neuropsychiatr Electrophysiol, 2 (6) (2016)

Merrin EL, Floyd TC. Negative symptoms and EEG alpha in schizophrenia: a replication. Schizophr Res. 1996; 19(2–3):151–61

Miyata J, Sasamoto A, Koelkebeck K, Hirao K, Ueda K, Kawada R, et al. Abnormal Asymmetry of White Matter Integrity in Schizophrenia Revealed by Voxelwise Diffusion Tensor Imaging. Human Brain Mapping 2012; 33:1741–1749. doi: 10.1002/hbm.21326

Moran LV, L.E. Hong.High vs low frequency neural oscillations in schizophrenia Schizophr Bull, 37 (2011), pp. 659-663

Oertel-Knoechel V, Knoechel C, Staeblein M, Linden DE. Abnormal Functional and Structural Asymmetry as Biomarker for Schizophrenia. Current Topics in Medicinal Chemistry 2012; 12(21): 2434–2451.

Olejarczyk, E, Jernajczyk, W. Graph-based analysis of brain connectivity in schizophrenia. PLoS One. 2017;12:e0188629. doi:10.1371/journal.pone.0188629

Ragland JD, Yoon J, Minzenberg MJ, Carter CS. Neuroimaging of cognitive disability in schizophrenia: Search for a pathophysiological mechanism. Int Rev Psychiatry 2007; 19(4): 417–427. doi: 10.1080/09540260701486365

Ribolsi M, Daskalakis ZJ, Siracusano A, Koch G. Abnormal asymmetry of brain connectivity in schizophrenia. Frontiers in Human Neuroscience 2014; 8: 1010
doi: 10.3389/fnhum.2014.01010

Roffo, G., Melzi, S. and Cristani, M., 2015. Infinite feature selection. In Proceedings of the IEEE International Conference on Computer Vision (pp. 4202-4210).

Schmitt A, Hasan A, Gruber O, Falkai P. Schizophrenia as a disorder of disconnectivity. Eur Arch Psychiatry Clin Neurosci. 2011; 261 Suppl 2:S150–4.

Sharp FR, Hendren RL. Psychosis: atypical limbic epilepsy versus limbic hyperexcitability with onset at puberty? Epilepsy Behav 10: 515–520, 2007

Shenton ME, Dickey CC, Frumin M, McCarley RW. A review of MRI findings in schizophrenia. Schizophr Res. 2001; 49(1–2): 1–52.

Tamminga CA, Stan AD, Wagner AD. The hippocampal formation in schizophrenia. Am J Psychiatry 167: 1178–1193, 2010

Tauscher J, Fischer P, Neumeister A, Rappelsberger P, Kasper S. Low frontal electroencephalographic coherence in neuroleptic-free schizophrenic patients. Biol Psychiatry. 1998;44(6):438–47.

von Stein A, Sarnthein J. Different frequencies for different scales of cortical integration: from local gamma to long range alpha/theta synchronization. Int. J. Psychophysiol. 2000; 38: 301–313.

Winterer G, Egan MF, Radler T, Hyde T, Coppola R, Weinberger DR. An association between reduced interhemispheric EEG coherence in the temporal lobe and genetic risk for schizophrenia. Schizophr Res. 2001;49(1–2):129–43.

Zhang Y, T. Yoshida, D.B. Katz, J.E. LismanNMDAR antagonist action in thalamus imposes delta oscillations on the hippocampus J. Neurophysiol., 107 (2012), pp. 3181-3189

Zhang Y, H. Zhang, X. Chen, S.-W. Lee, D. ShenHybrid high-order functional connectivity networks using resting-state functional MRI for mild cognitive impairment diagnosis. Scientific Reports (2017)